Transport, magnetic and thermal properties of Pr doped $LaSr_2Mn_2O_7$: a Kondo-type behaviour of resistivity

2006 J. Phys.: Condens. Matter 18 7179

(http://iopscience.iop.org/0953-8984/18/31/013)

INSTITUTE OF PHYSICS PUBLISHING JOURNAL OF PHYSICS: CONDENSED MATTER

J. Phys.: Condens. Matter **18** (2006) 7179–7192 doi:10.1088/0953-8984/18/31/013

Transport, magnetic and thermal properties of Pr doped $LaSr_2Mn_2O_7$: a Kondo-type behaviour of resistivity

S N Bhatia[1], Niharika Mohapatra[1], Darshan Kundaliya[2] and S K Malik[2]

[1] Department of Physics, Indian Institute of Technology, Powai, Mumbai 400 076, India
[2] Tata Institute of Fundamental Research, Colaba, Mumbai 400005, India

Received 29 March 2006, in final form 21 June 2006
Published 21 July 2006
Online at stacks.iop.org/JPhysCM/18/7179

Abstract

The interplay of spin, charge and lattice degrees of freedom in $LaSr_2Mn_2O_7$ (tetragonal, space group $I4/mmm$) yields a variety of properties such as a CE-type charge ordering and an A-type spin ordering. We have studied the effect of partial replacement of La by Pr on the magnetic and thermal properties of this system. Compounds of the type $La_{1-x}Pr_xSr_2Mn_2O_7$ ($0 \leqslant x \leqslant 1$) have been prepared and are found to crystallize in the same tetragonal structure. Magnetization, electrical resistivity and specific heat measurements have been carried out on these compounds. Replacing La by Pr in this system affects both the electronic and the magnetic state of the system. It is observed that the charge ordering temperature and the net magnetic moment reduce with the incorporation of Pr in the lattice. In the antiferromagnetic state, the charge carriers in $La_{1-x}Pr_xSr_2Mn_2O_7$ behave like a weakly scattered two-dimensional gas whose resistivity (ρ) is a logarithmic function of temperature, T ($\rho \propto \log T$), over a certain temperature interval. This behaviour is enhanced with increasing concentration of Pr in the samples and is proposed to originate from quantum interference. The electronic part of the specific heat shows the presence of the two transitions at T_{CO} and T_N and a contribution from antiferromagnetic magnons at low temperatures.

1. Introduction

Recently, extensive experimental and theoretical investigation has been devoted to understanding the colossal magnetoresistance (CMR) effect around the ferromagnetic transition temperature (T_C) in doped manganites ($R_{1-x}A_xMnO_3$) having a perovskite structure where a strong interplay between charge, lattice, spin and orbital degrees of freedom yields a rich phase diagram [1–3]. The basic physics of these manganites is well understood in terms of the Hund's rule coupling between the e_g conduction electrons and the t_{2g} core electrons and the Jahn–Teller effect due to the presence of the Mn^{3+} ions [4]. At low temperatures, though the transport

is predominantly by free carriers, a weak localization giving a semiconducting behaviour is present in some of these manganites. Recently a Kondo-type effect, where the resistivity attains a minimum and then follows a logarithmic dependence on temperature at lower temperatures, has been observed in the ferromagnetic state for some compositions [5–7].

In the bilayered manganites $La_{2-2x}Sr_{1+2x}Mn_2O_7$, a MnO_2 bilayer is alternately stacked with a $(La, Sr)_2O_2$ rock salt layer along the c-axis. Neutron diffraction studies [8, 9] on the half-doped ($x = 0.5$) bilayered system $LaSr_2Mn_2O_7$ have revealed an ordering of the $d_{3x^2-r^2}/d_{3y^2-r^2}$ orbitals of the Mn ions accompanied by a real space ordering of Mn^{3+}/Mn^{4+} below the charge ordering temperature (T_{CO}) $\sim$ 210 K. The charge and orbital ordering (CO/OO) melts partially and an in-plane FM order with an inter-plane antiferromagnetic (AFM) coupling called the A-type antiferromagnetic phase together with a CE-type antiferromagnetic phase appear below $T_N \sim 180$ K. These phases coexist and the proportion of the former phase over the latter increases as the system is cooled below T_N. The physical properties of these bilayered manganites $La_{2-2x}Sr_{1+2x}Mn_2O_7$ strongly depend on the hole doping level x [10]. As Pr can exist in two different valence states Pr^{3+} and Pr^{4+}, Pr substitution therefore provides an easy way to study the entire phase diagram in the hole space. This relatively easy procedure for studying the entire phase diagram has not been exploited so far.

Though the electric conduction in the end member $PrSr_2Mn_2O_7$ has been studied recently [11], these results do not agree with the existing understanding of the CMR effect. These authors have shown that $PrSr_2Mn_2O_7$ remains an insulator down to the lowest temperature measured, but its magnetoresistance (MR) decreases in comparison to the MR in the parent composition. This contradicts the results observed for 3D manganites where the MR was seen to increase with Pr substitution [12]. An added motivation for these studies was a desire to see whether Pr substitution in $LaSr_2Mn_2O_7$ produced magnetic memory effects similar to those observed in $(La_{0.4}Pr_{0.6})_{1.2}Sr_{1.8}Mn_2O_7$ [13]. We have investigated the properties of $La_{1-x}Pr_xSr_2Mn_2O_7$ by systematically varying the Pr concentration, $0 \leqslant x \leqslant 1$. We find the localization of the charge carriers to increase upon this substitution. For all Pr concentrations, $0 \leqslant x \leqslant 1$, the resistivity and thermoelectric power (TEP) follow Mott's variable range hopping (VRH) model in the high temperature region (above $\sim$200 K). A second maximum in resistivity at temperatures below the maximum produced by the antiferromagnetic ordering is observed. The resistivity follows a $\log T$ type of behaviour over some temperature interval between the two maxima. This behaviour appears to evolve with increasing Pr concentration and is attributed to the increase in the localization produced by Pr. The MR was observed to increase with increasing Pr concentration, but no dramatic increase in its value was observed at any Pr concentration. Though irreversibility is observed in the magnetization, ac susceptibility does not show any spin glass effect. The heat capacity shows two transitions at T_{CO} and T_N and a contribution from free electrons in the intermediate temperature range and another from antiferromagnetic magnons at low temperatures.

2. Experimental procedures

Standard solid-state ceramic techniques were employed to synthesize the polycrystalline samples with the compositions $La_{1-x}Pr_xSr_2Mn_2O_7$ ($0 \leqslant x \leqslant 1.0$). Stoichiometric amounts of pure ($\geqslant$99.9%) La_2O_3, Pr_6O_{11}, MnO_2 and $SrCO_3$ were properly mixed and fired four times at temperatures in the range 950–1350 °C. Rectangular shaped pallets were used for the final sintering which was carried out in air at 1400 °C. The phase purity was examined by Philips PW3710 diffractometer with Cu Kα radiation. Electrical resistivity (ρ) was measured by the standard four-probe technique in the temperature range of 10–300 K in a closed-cycle refrigerator. The seesaw heating method [14] was employed for the measurement of

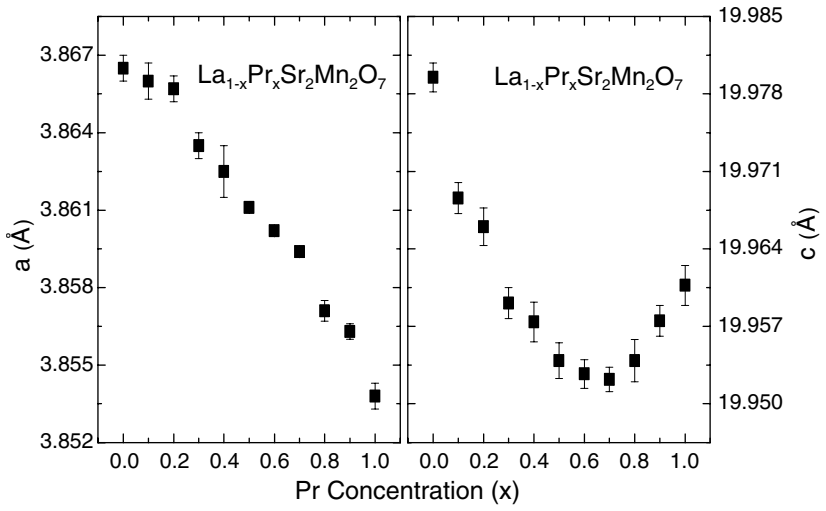

Figure 1. The variation of the lattice constants a and c of $La_{1-x}Pr_xSr_2Mn_2O_7$ with the Pr concentration.

the thermoelectric power (TEP). In this technique two identical heaters (strain gauges) were mounted on the two ends of the sample. By alternating the heat between the two ends of the sample, spurious voltages generated there could be cancelled. Copper–constantan thermocouples above 100 K and gold–iron ones below this temperature were used for the measurements of all thermal voltages. Magnetization measurements were performed using a SQUID Magnetometer (Quantum Design, MPMS). Magnetization data for both field cooled (FC) and zero-field cooled (ZFC) modes were collected at a constant field of 5 mT. The magnetoresistance and heat capacity measurements were carried out in zero and 8 T fields (PPMS, Quantum Design).

3. Results and analysis

The x-ray diffraction patterns, recorded at room temperature, confirmed all samples, $La_{1-x}Pr_xSr_2Mn_2O_7$ ($0 \leqslant x \leqslant 1.0$), to form in single phase without any detectable impurities. Reitveld profile refinement software was used to determine the lattice constants and other structural parameters. The crystal structure and symmetry do not change with Pr doping which remains tetragonal with space group $I4/mmm$. As shown in figure 1, the lattice constant a decreases with increasing Pr concentration up to $x = 1$ while c decreases initially, forms a trough around $x \sim 0.5$ and then increases for $x \geqslant 0.7$ only. However the volume of the unit cell continues to decrease with increasing Pr concentration.

The ESCA spectrum for the composition $La_{0.3}Pr_{0.7}Sr_2Mn_2O_7$ is presented in figure 2. Two distinct peaks at the binding energies 933.1 and 951.0 eV are observable corresponding to the spin–orbit splitting of the 3d state into $3d_{5/2}$ and $3d_{3/2}$ states. For comparison, the spectrum of Pr_6O_{11} is also given where two peaks at the same binding energies are observed. As shown in the figure, two Gaussian lines, centred at the energy values 933.04 and 935.27 eV, are required to reproduce the $3d_{5/2}$ peak of Pr_6O_{11}. These values are close to the binding energies of the Pr^{3+} and Pr^{4+} states. However the data for our sample ($La_{0.3}Pr_{0.7}Sr_2Mn_2O_7$) can be fitted well to a *single* Gaussian line with energy 933 eV. A similar result is obtained for all the Pr concentrations. This shows that Pr is present in the 3+ state *only* for all Pr concentrations. As

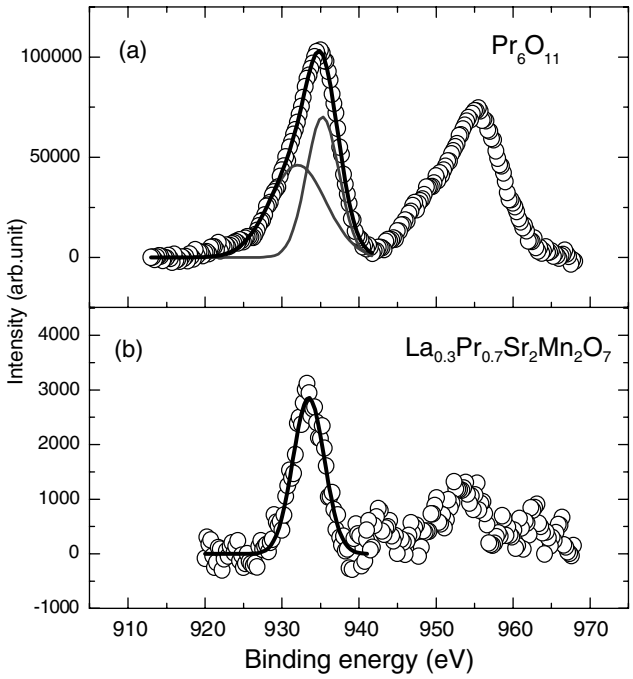

Figure 2. (a) The ESCA spectrum of Pr_6O_{11}. The solid curve is calculated with two Gaussian lines. (b) The ESCA spectrum of $La_{0.3}Pr_{0.7}Sr_2Mn_2O_7$. The peak here is fitted to a single Gaussian line.

this valence of Pr is the same as that of La, this means that the addition of Pr to $LaSr_2Mn_2O_7$ does not increase the carrier density in these samples. The idiomatic titrations of these samples (with $x = 0.3$, 0.5 and 0.7) also gave the average valence of Mn ions to be 3.46 ± 0.1, further confirming the carrier density to remain essentially unchanged with the addition of Pr. It must be pointed out that with the addition of Pr, the oxygen content of a formula unit generally increases slightly above the value governed by the stoichiometry of the formula. These additional oxygen ions suck electrons from the metallic ions in the formula unit in order to properly bond themselves within the network. The Mn valence quoted above was calculated for a stoichiometric formula. However deviations from stoichiometry will reduce the valence by $\sim$10% which will not affect the argument given above.

4. Magnetization

Figure 3 shows the magnetization, $M(T)$, measured in a field of 5 T as a function of temperature for all Pr concentrations. As in the parent composition, a broad peak around $\sim$210 K is seen in the magnetization of all Pr concentrations but the data cannot be used to resolve the two transitions at T_{CO} and T_N. The increase in the widths of these peaks with x shows the distribution of the exchange interactions in the Mn–O–Mn network to broaden with increasing Pr concentration in the samples. The ac susceptibility, measured in a field of $\sim$0.5 mT at 33 Hz, also does not show a sharp transition at T_N for any sample. Instead a hump is seen in this temperature range for all the samples. The hump reduces in height and increases in width with increasing x. Addition of Pr reduces the magnetization at all temperatures. Also in this plot a cusp is seen at $\sim$20 K for samples with Pr concentrations $x \geqslant 0.7$ which may arise from

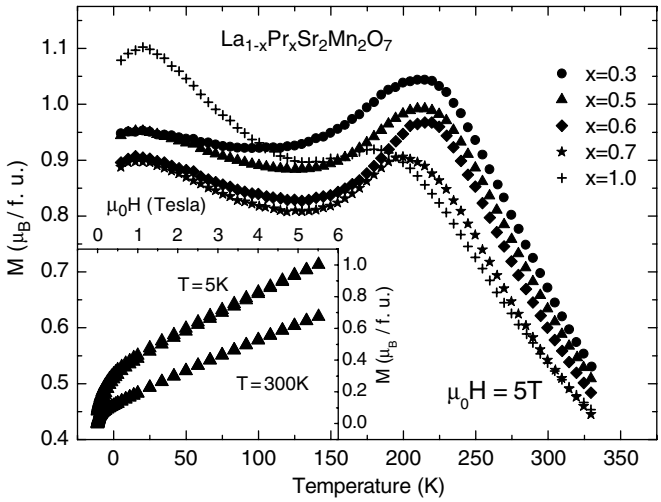

Figure 3. The main panel shows the magnetization of $La_{1-x}Pr_xSr_2Mn_2O_7$ measured at 5 T. Its variation with field at two temperatures is shown in the inset for a representative concentration ($x = 0.5$).

the ordering of the Pr moments, as has been seen earlier for $Pr_{0.7}Ca_{0.3}MnO_3$ [15] also. For the $x = 1$ sample, i.e. $PrSr_2Mn_2O_7$, a plateau is observed below T_N as against the drop observed for other Pr concentrations.

The zero-field cooled (ZFC) and field cooled (FC) magnetizations measured in 5 mT are shown in figure 4. Both curves show a peak around T_{CO}. As shown in figure 3 the (saturation) magnetization at ∼5 K, obtained from both the (FC and ZFC) curves, decreases with increasing Pr concentration up to $x \sim 0.6$, and becomes independent of x above this value ($0.7 \leqslant x \leqslant 0.9$). At high fields (5 T) also (figure 3), $M(T)$ curves for $0.7 \leqslant x \leqslant 0.9$ are seen to merge with each other at low temperatures. The FC and ZFC curves bifurcate right below the room temperature. The ratio of the two magnetizations, $M_{FC}/M_{ZFC} = m$, remains near ∼1 down to T_{CO} and then shoots to high values upon further cooling; figure 4. The bifurcation does not result from the spin glass (SG) type of freezing of the moments as a cusp is not seen in the ac susceptibility in this temperature region. (The temperature of the maximum of the hump appears to be frequency independent though it could not be ascertained unambiguously due to the large width of the hump.) Sheshadri *et al* [16] also did not see any spin glass effect in the parent compound. As a function of field, the magnetization increases rapidly at low fields and varies linearly with field above ∼1 T at all temperatures. This is shown in the inset of figure 3 for one concentration $x = 0.5$, i.e. $La_{0.5}Pr_{0.5}Sr_2Mn_2O_7$, at 5 and 300 K. The magnetization does not saturate at low temperatures with the highest field used (6 T). This behaviour points towards the absence of a true long range order below T_N. For the parent compound one of the authors [17] had shown earlier, from the deviations of the high temperature dc susceptibility from the Curie–Weiss law below ∼480 K, that above T_{CO} the system was present in the Griffiths phase in which FM clusters of varying size formed and grew upon cooling. Our MR data on these samples (given below) also show clusters to be present above T_{CO} in the Pr containing samples. It is probable that these clusters continue to grow upon cooling, undergo an antiferromagnetic transition at T_N and together with the zigzag chains of the insulating CE phase give an inhomogeneous AFM state below T_N.

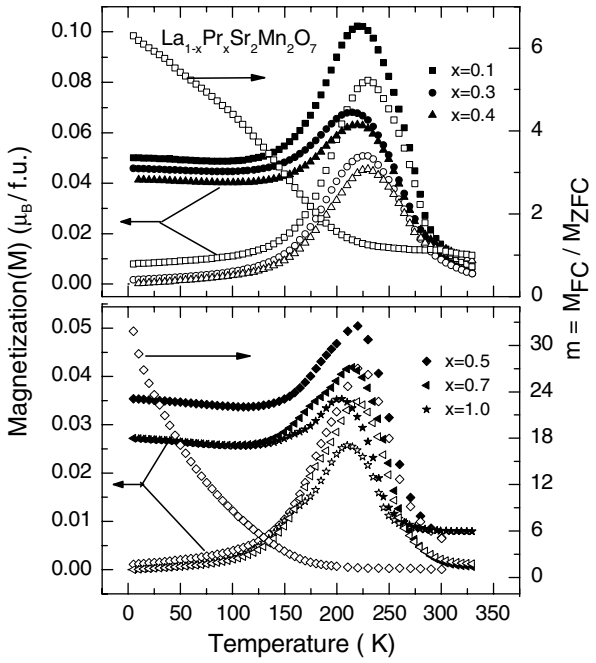

Figure 4. The temperature variation of the FC (closed symbols) and ZFC (open symbols) magnetization of $La_{1-x}Pr_xSr_2Mn_2O_7$ and their ratio m. The field used here is 5 mT. m is plotted for the $x = 0.1$ and 0.5 samples in the upper and the lower panels respectively.

5. Resistivity and thermopower above $T_N(x)$

The temperature dependence of the resistivity of $La_{1-x}Pr_xSr_2Mn_2O_7$ with $0.0 \leqslant x \leqslant 1.0$ is presented in figure 5. Though qualitatively the resistivity behaviour for all Pr concentrations is similar to that of the parent composition, some new features appear at higher Pr concentrations. Around ∼200 K all the compositions show a maximum at $T_{\max 1}(x)$, but a second maximum appears at a lower temperature $T_{\max 2}(x)$ at higher concentrations of Pr. For the parent composition the maximum at $T_{\max 1}$ (∼180 K) is sharp, but for the doped samples both maxima are very shallow and therefore difficult to resolve on small plots. However the derivative $d\rho/dT$ varies sharply with T near $T_{\max 1}$ and consequently the derivative plots, $d\rho/dT$ versus T, help in its resolution in all the samples. As seen in all the curves shown in the inset of figure 5, $d\rho/dT$, after a gradual change, starts to increase abruptly in magnitude *below* ∼200 K and then turns around at a temperature near $T_{\max 1}$. The turnaround in $d\rho/dT$ curves suggests a positive contribution being added to $d\rho/dT$. In the parent compound charge ordering produces an abrupt increase in resistivity while the spin ordering facilitates the double-exchange (DE) interaction between the Mn ions due to which the conductivity increases. The downward increase in $d\rho/dT$ decreases and eventually the $d\rho/dT$ curve turns upwards. The temperature of the minimum in $d\rho/dT$ coincides with that of the maximum in the resistivity and T_N determined from neutron diffraction experiments. As the $d\rho/dT$ versus T curves look similar for all x ($0 \leqslant x \leqslant 1$) the processes occurring in these compositions must also be identical. $T_{\max 1}$ in each Pr containing sample can then be identified as its T_N and the temperature (above $T_{\max 1}$) where the slope of the $d\rho/dT$ curve changes abruptly as T_{CO}, though the latter criterion is subjective. It is seen from these curves that with the addition of Pr both these

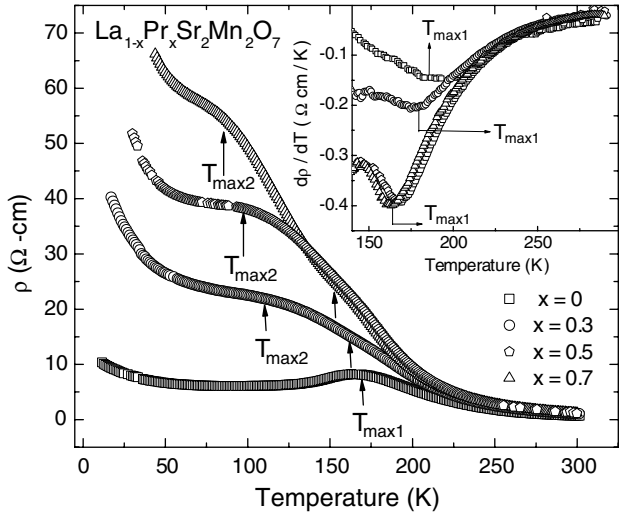

Figure 5. The resistivity of $La_{1-x}Pr_xSr_2Mn_2O_7$ varying with temperature. Only four concentrations are shown for clarity. The temperatures where $\rho(T)$ attains maxima are shown by arrows. The inset shows the derivative $d\rho/dT$ as a function of temperature. It highlights the presence of a maximum in $\rho(T)$ at $T_{max\,1}$ in Pr containing samples.

temperatures, T_{CO} and T_N, decrease slightly. As shown in the inset of figure 7, with increasing Pr concentration, $\rho(T)$ increases with x for all x below T_{CO}, but above this temperature it decreases suddenly in its value around $x \sim 0.6$. Also a hysteretic behaviour observed in the resistivity of the parent compound between 70 and 170 K reduces with x and finally disappears for $x > 0.5$.

The thermoelectric power (TEP) of $La_{1-x}Pr_xSr_2Mn_2O_7$ is shown in figure 6 for some selected concentrations. For all concentrations it increases upon cooling, though it remains negative over the entire temperature range 20–300 K and does not show hysteresis upon thermal cycling. The TEP becomes more negative as the Pr concentration increases, which again points towards a reduced conduction.

In the temperature region (∼200–300 K), the semiconducting behaviour of the resistivity of the parent compound ($La_1Sr_2Mn_2O_7$) could be explained in terms of Mott's variable range hopping (VRH) model [18]:

$$\rho = \rho_\infty \exp\left[\frac{T_0}{T}\right]^\nu \tag{1}$$

with $\nu = 1/3$ where ν equals 1/3 and 1/4 for hopping in two and three dimensions respectively and T_0 is the Mott activation energy. $T_0 \propto 1/N(E_f)\xi^2$ where $N(E_f)$ is the density of states at the Fermi level and ξ the localization length. Under similar conditions, TEP is expected to vary as T^μ with $\mu = 1/3$ and 1/2 for the respective dimensions of hopping. For the doped samples, the model agrees equally well with the resistivity data for both values of ν. However the TEP data accept the former value of μ, namely 1/3 only, as shown in the inset of figure 6. For some Pr concentrations, plots of $\log\rho$ versus $T^{-1/3}$ are shown in figure 7 and are seen to be straight. As happens frequently in these studies, the resistivity data also follow this equation with $\nu = 1/2$ corresponding to the hopping with the Coulomb gap (HCG) in the density of states. However, on this model TEP is predicted to be temperature independent [19] which is not observed here. The other conduction behaviours commonly observed in such materials, namely the thermally activated hopping ($\rho(T) = \rho_0 \exp(E_\rho/k_B T)$) and small polaron hopping

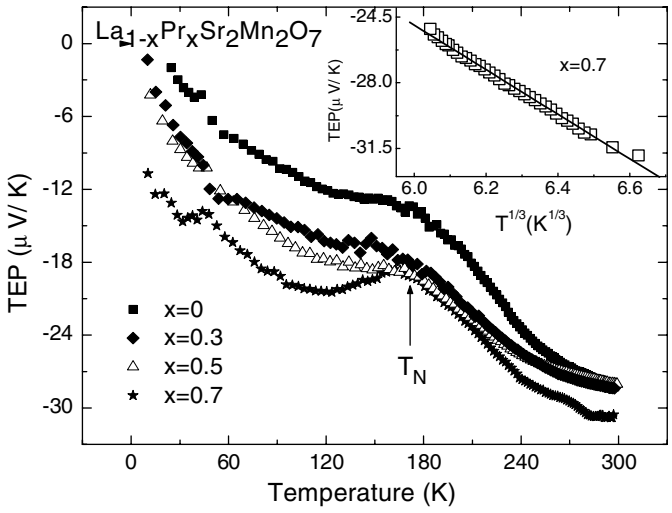

Figure 6. Thermopower of $La_{1-x}Pr_xSr_2Mn_2O_7$ for various Pr concentrations. The inset shows that the TEP follows the 2D VRH model for conduction above ∼200 K.

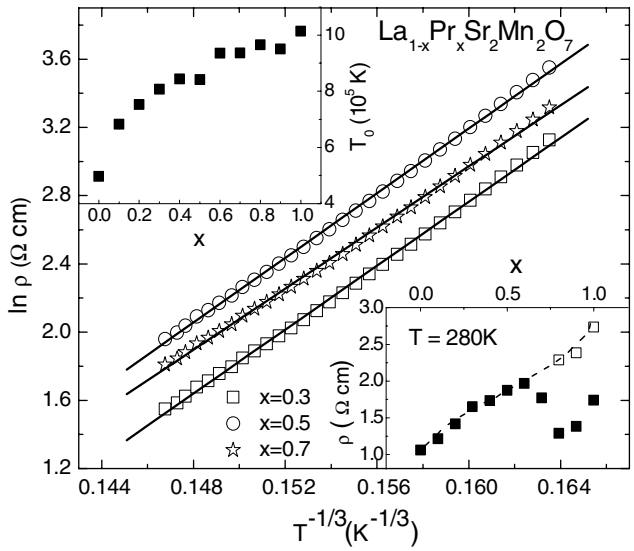

Figure 7. Linear plots of ln ρ versus $T^{-1/3}$ showing conduction to follow Mott's VRH model. The upper inset shows that the characteristic temperature T_0 increases with x while the lower inset shows that the room temperature resistivity increases with Pr concentration (dotted curve) with a sudden drop at $x = 0.6$.

$(\rho(T) = \rho_0 T \exp(E_\rho/k_B T))$, could also be discounted as a temperature independent activation energy (E_ρ) could not be obtained from the resistivity data. Moreover the TEP for these activated processes is predicted to vary as $Q(T) = (k_B/e)(E_Q/k_B T) + Q_\infty$ with the activation energy $E_Q \ll E_\rho$. However our TEP data failed to give a linear plot of Q versus $1/T$ for any of the Pr concentrations. Thus the transport data suggest unambiguously that the conduction takes place by hopping of the carriers to different sites within the Mn–O planes for all Pr concentrations, $0 \leqslant x \leqslant 1.0$. T_0 increases with x as is seen in figure 7 (upper inset). As a

consequence, the minima in $d\rho/dT$ get more pronounced (see the inset in figure 5). Assuming the $N(E_f)$ to remain unchanged with x, this indicates a decrease in the localization length, which makes the material less conducting.

From the inset of figure 7 it is seen that if the resistivity for $x > 0.7$ is scaled up, then ρ over the entire concentration range follows a smooth curve (shown dotted) with a sharp drop at $x \sim 0.6$. At this concentration the lattice parameter also starts to increase with x (figure 1). Thus it appears that the primary effect of Pr substitution is to increase the resistivity and the change in the chemical pressure accompanying this substitution produces the sharp drop in its value at $x \sim 0.6$. In other oxides also, Pr substitution increases the resistivity [20]. From the analysis of the XRD data, we find the in-plane Mn–O bond length, d_{in}, to decrease with x for $0 \leqslant x \leqslant 1$ while the out-of-plane Mn–O bonds, d_{out}, show a reversal in the decrease in their values around $x \sim 0.6$. The JT distortion consequently increases rapidly around this Pr concentration. Neutron diffraction results for $La_{1-x}Nd_xSr_2Mn_2O_7$ [21] show the d_{in} and d_{out} to vary smoothly with Nd concentration where a and c also vary smoothly with x. A similar drop in resistivity is observed in the bilayer system $La_{1.2}Sr_{1.8}Mn_2O_7$ which undergoes an insulator to FM metal transition at 120 K. The c-axis length in this system also decreases up to 120 K and then increases on further cooling [22]. Mitchell *et al* [22] have shown that the changes in the lattice parameters at 120 K are accompanied by an increase in the Jahn–Teller distortion, Δ, at this temperature.

The random potential that localizes the carriers has a predominant magnetic contribution arising from the Hund's rule coupling between the e_g conduction electrons and the t_{2g} core electrons of the Mn ion. Though Pr does not alter the Coulomb potential in the lattice, being isovalent with La, its 4f electrons influence the orientation of the t_{2g} spins as the magnetization of these samples is observed to vary with Pr concentration in the paramagnetic state. Consequently the spin dependent potential fluctuates due to the presence of Pr. These fluctuations may attain a large value near the Pr sites. The e_g electrons can then be trapped at these sites. As suggested by Coey *et al* [23], together with the JT distortion the random fluctuations of the spin dependent potential are likely to produce an immobile large magnetic polaron. Conduction then takes place by hopping of the electron from one wavepacket to another across the potential barrier at the Pr site.

5.1. Magnetoresistance

Application of a magnetic field decreases the resistivity of all the samples throughout the temperature range investigated. Considerable hysteresis is observed in field cycling the resistivity at low temperatures. As shown in figure 8, at 300 K, the $\rho(T, H)/\rho(T, 0)$ versus H curves obtained with increasing and decreasing field coincide, but below T_N they separate. The irreversibility increases with increasing Pr doping level. The charge ordering does not melt up to 8 T for all Pr concentrations. T_N shifts to higher temperatures with field and varies at a rate $\sim$0.4 K T^{-1} for all x. MR $(=(\rho(0) - \rho(H))/\rho(0))$ increases as the samples become more resistive with increasing Pr concentration. As shown in the inset of figure 8, it also increases with decreasing temperature. Like the resistivity, MR also shows a break in slope around $T_{max\,2}$ of the composition.

The field dependence of MR above T_{CO} provides another opportunity to further understand the hopping mechanism. The field reduces the disorder and consequently the spin dependent part of the random potential experienced by the hopping carriers. The reduced barrier heights still do not permit thermally activated hopping by the carriers as plots of $\log \rho(T, H)$ versus $1/T$ still show considerable curvature. Viret *et al* [24] have calculated the effect of the spin disorder on hopping. They find that in the presence of this disorder, the conduction continues

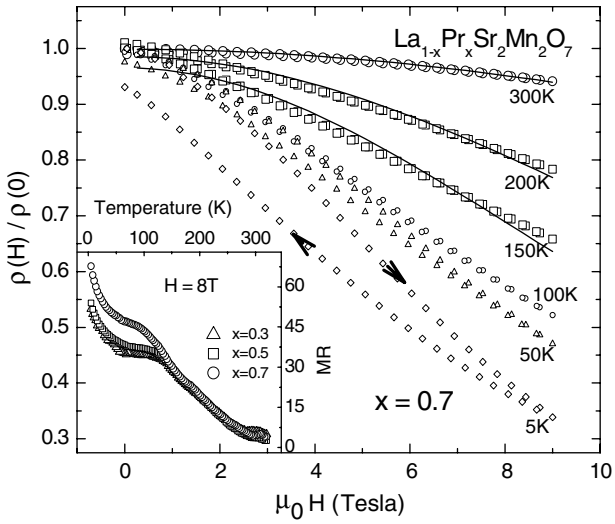

Figure 8. The resistivity decreasing with field at all temperatures for the $x = 0.7$ sample. The hysteresis with field cycling increases with decreasing temperature. The solid curves through the data are calculated from the Viret *et al* model. The agreement with the model appears to deteriorate as the temperature approaches T_N. The inset shows the temperature variation of MR.

to be governed by equation (1), with T_0 modified to

$$T_{0H} = T_0 \left(1 - \left(\frac{M(T)}{M_S}\right)^2\right) \tag{2}$$

where M_S is the saturation magnetization of the sample. The ratio $M(T)/M_S$ in an applied field H can be related to the Brillouin function B_S $(g\mu_B SH/k_B T)$ within the framework of molecular field theory. Here S represents the spin of the scattering entity. Therefore it follows from this equation that the logarithm of the resistivity ratio $\rho(H, T)/\rho(0, T)$ should vary as $(1 - B_S^2)^\nu$ at a constant temperature in the paramagnetic region with H as the externally applied field. The solid curves in figure 8 show the results of these calculations obtained with $\nu = 1/3$ and $S \sim 9$. The agreement is satisfactory above T_{CO} but deteriorates as T_N is approached. Such a large value of S suggests the spins to be clustering together. A similar clustering of the spins was seen in the high temperature susceptibility of the parent composition [17]. T_0 obtained from these fits also agrees with its value obtained from the zero-field resistivity data.

6. Resistivity and thermopower below $T_N(x)$

Over some temperature interval between $T_{max\,2}$ and $T_{max\,1}$, the resistivity is observed to vary with temperature as a logarithmic function of temperature ($\rho \propto \log T$), figure 9, with a slope $(=\partial\rho/\partial \ln T)$ that increases with increasing x. The $\log T$ behaviour is not seen in the parent composition where below $T_{max\,1}$ the resistivity shows a rather flat and shallow minimum and then continues to increase up to the lowest temperature, but it can be clearly seen at higher Pr concentrations where the temperature interval of its occurrence is large. The $\log T$ behaviour appears to evolve with Pr as the temperature interval over which it is observed increases as x increases. The observed $\log T$ behaviour is reproducible over many samples prepared in different batches.

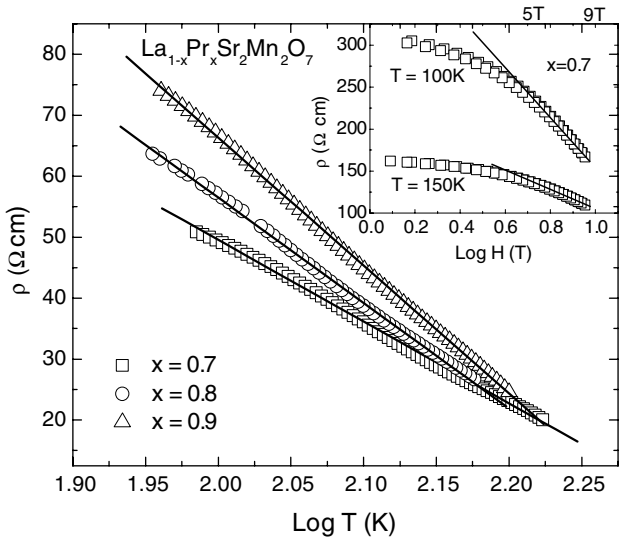

Figure 9. The $\log T$ behaviour of $\rho(T)$ of some Pr containing samples in a small temperature interval above $T_{\max 2}$. The upper inset shows the $\log H$ dependence of ρ on the field. The lower inset shows the variation of the Mott parameter T_0 with the Pr concentration.

A $\log T$ dependence of ρ below a resistivity *minimum* is characteristic of the Kondo effect in dilute magnetic systems in which the free electrons are scattered from the *isolated* magnetic ions. Recently a resistance *maximum* followed by a $\log T$ behaviour at higher temperatures was observed in concentrated Kondo systems such as $La_{0.1}Ce_{0.4}Sr_{0.5}MnO_3$ [25] and attributed to Ce^{3+} undergoing a transition to the mixed valence Ce^{3+}/Ce^{4+} state. Though Pr can also exist in two valence states, it is not known to produce the Kondo effect in manganites and cuprates. Some strongly disordered crystalline and amorphous alloys such as Cu–Ti, Cu–Zr, Ni–Zr, Fe–Ni and $(La, Pd_3)_8Mn$ [26] also show a $\log T$ behaviour in resistivity. They also have high resistivity ($>200\ \mu\Omega$ cm) and a negative TCR as observed for the samples under study. The $\log T$ behaviour of these amorphous samples arises due to the quantum interference effects [27]. The forward moving carrier waves interfere with those scattered by the random potential of the impurities and this leads to phase coherence between the scattered waves. As a consequence the probability of an electron returning to its origin is increased which implies a tendency towards localization. This tendency is further enhanced by some quantum effects [28]. Lee and Ramakrishnan [29] have shown the conductivity of a gas of such localized non-interacting carriers weakly scattered by rigid random impurities to be given by $\frac{p}{2}\frac{e^2}{\pi^2\hbar}\log(T/T_0)$ when the gas is two dimensional and $\frac{e^2}{\pi^3\hbar}\frac{1}{a}T^{p/2}$ when it is three dimensional (the index p depends on the dominant scattering mechanism and generally $1 < p \leqslant 2$, a is the material length and T_0 is a constant). The localization effects are weakened by the magnetic field. At fields where the dephasing length becomes smaller than the diffusion distance of the carriers, the resistivity is expected to vary with the field as $\log H$. We propose that the $\log T$ behaviour observed here arises from the quantum interference as, in addition to the $\log T$ behaviour, the resistivity in the present compositions varies as $\log H$ above $\sim$5 T (figure 9, inset). As mentioned above, the onset of antiferromagnetism delocalizes the carriers in systems having DE interactions. The carriers may be relocalized by the fluctuations in the spin dependent potential which localized the carriers above T_{CO}. These fluctuations are present in the AFM state also, as the influence

of Pr on the alignment of the Mn spins is still present. These may further be enhanced by the inhomogeneity of the AFM state. Localization enhances the magnetoresistance. Though the magnetoresistance increases with x in the samples under study, this cannot be taken as evidence for the presence of the localization as the DE interaction present in the samples is expected to give a large MR that may outweigh the contribution coming from it.

A $\log T$ behaviour of resistivity also arises in a gas of interacting electrons where the electron–electron interaction arises from the modified Coulomb interaction between electrons weakly localized by impurity scattering. As the ESCA analysis has shown that the carrier density remains unchanged with the addition of Pr, so the el–el interaction remains at the level present in the parent compound and consequently is not expected to yield the $\log T$ dependence of ρ in Pr containing samples. Moreover $\rho(T, H)$ for interacting electrons is expected to vary as $\sqrt{H}$ which is not observed for any composition.

Quantum interference drastically reduces the conductivity in 2D systems while it has a marginal effect in 3D systems. For example this correction to conductivity is $\sim 10^5$ Ω m in the 3D systems whereas it works out at $\sim 10^{-5}$ Ω^{-1} only for the 2D systems. Consequently it is readily observable in the ferromagnetic phase of the 3D manganites where the resistivity is low. Together with the inelastic scattering of the carriers from the lattice excitations it produces a resistivity minimum at low temperatures which is observed in some perovskite manganites. The layered manganites on the other hand are highly resistive due to the low dimensionality of the layer carrying the carriers. The quantum correction further increases this resistivity.

Below $T_{\max 2}$ the resistivity decreases. Though it passes through a minimum around $\sim$100 K for all concentrations, it does not show the $\log T$ dependence for any x. Below 100 K, the data follow equation (1) for all Pr concentrations but the corresponding T_0 decreases by three orders of magnitude from its high temperature value. Consequently ξ increases to $\sim$120 Å. With such a large ξ, the carriers cannot be considered as localized.

7. Specific heat

Figure 10 shows the specific heat, C_P, versus temperature plots for some representative samples at 0 T. C_P is essentially independent of the field throughout the temperature range as the measurements at 9 T coincide with the zero-field values. C_P varies smoothly with temperature through all the transitions. Only near $T_{\rm CO}$ is there a hint of a transition as the slope of the curve changes around this temperature. This behaviour contrasts sharply with that observed for perovskite manganites where C_P displays a huge peak at $T_{\rm CO}$. Below $\sim$10 K, C_P agrees with $C_P = AT^3 + \gamma T + \beta T^m$. The second term represents the contribution from the free electrons and the third the magnetic contribution arising from the magnon gas. For ferromagnetic magnons, m equals one and 3/2 for the 2D and 3D magnon gas respectively and 2 and 3 for the AFM magnons of the same dimensions. The best agreement is obtained for $\gamma \sim 0$ and $m = 2$ (upper inset in figure 10). Allowing m to vary freely, β becomes negative as soon as m comes close to the value one. Thus the 2D AFM magnons dominate the thermal transport at low temperatures. As noted above, below $\sim$50 K the resistivity of all the samples becomes very high. The movement of the electrons is severely restricted at these temperatures. A vanishing value of γ obtained from the C_P data is consistent with this inference.

The Einstein model together with a linear term and a quadratic term describes C_P adequately within 50 K $\leqslant T \leqslant$ 150 K. Only three frequencies corresponding to 117, 320 and 655 K were required. These frequencies are not related to the optical phonon modes seen in the IR spectra for this composition [30]. A finite value of the linear term obtained from the fitting implies that (free) electrons are present within this temperature interval. Though the linear term is usually used for a gas of free electrons, it is valid for the localized electrons

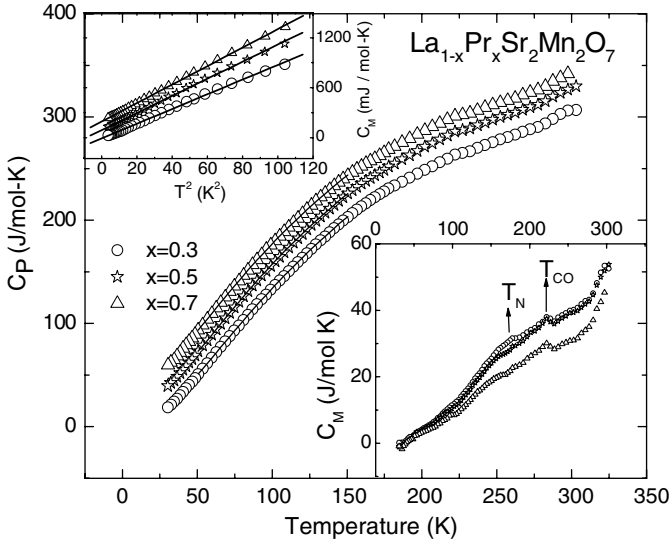

Figure 10. The specific heat data for $La_{1-x}Pr_xSr_2Mn_2O_7$ for some Pr concentrations. The solid lines represent the agreement with the various models at different temperatures discussed in the text. The upper inset shows the *magnetic* specific heat to originate from the 2D AFM magnons while in the lower inset the presence of the two transitions at T_N and T_{CO} is confirmed in the *non-phononic* part of the specific heat.

also, as for the equilibrium properties such as the specific heat and magnetization the difference between the localized and non-localized states is of no importance. So the localized electrons which gave the log T behaviour in resistivity will contribute the same γT term to C_P. However the el–el interaction yields different contributions to C_P depending on the dimensionality of the gas, namely log T and $a\sqrt{T}$ terms for 2D and 3D respectively. As the electronic contribution to C_P itself is quite small, the presence of this correction could not be ascertained unambiguously.

By assuming the same phonon frequencies to contribute to C_L above 150 K also, we have calculated the excess specific heat $\Delta C = C(T) - C_P$ produced by the non-phononic sources. Two small peaks are observed for the $x = 0.3$ sample at temperatures corresponding to T_{CO} and T_N as shown in figure 10 (lower inset). The peak at T_N is very broad and does not look like a λ-type anomaly. It decreases in height with increasing Pr concentration and becomes difficult to resolve for $x > 0.5$. The peak at T_{CO} does not dissolve up to the highest Pr concentration studied. Roughly 50, 76 and 90% of the spin entropy ($=2R\ln(2S+1)$ with $S = 3.75$) is gained up to 180, 210 K and the room temperature respectively for all concentrations of Pr. This shows a considerable amount of short range order to be present above T_N and that the SRO extends to temperatures much above room temperature.

8. Conclusions

We have investigated the transport, magnetic and thermal properties of Pr doped $La_{1-x}Pr_xSr_2Mn_2O_7$. In the paramagnetic phase we found ferromagnetic clusters to be present. Both the charge ordering temperature and the antiferromagnetic transition temperature decrease slowly with increasing x. In the paramagnetic state, the carriers hop within the Mn–O sheets and their localization increases with increasing Pr concentration. It is proposed that the Kondo-type behaviour in resistivity which is observed below T_N originates from the quantum

interference effects as the other possible origins of this effect, the spin glass and the electron–electron interactions, are not present here. The ac susceptibility shows the absence of the SG behaviour and the ESCA data discount any increase in the carrier density with the addition of Pr. Below T_N the carriers delocalized by the onset of antiferromagnetism appear to get relocalized by the fluctuations in the spin dependent potential. At low x, localization is not strong enough to produce an observable effect. Therefore the Kondo-type behaviour in resistivity is observed at higher Pr concentrations only.

Acknowledgments

We gratefully acknowledge the help provided by Professor B D Padalia in analysing the ESCA spectra of these samples.

References

[1] Kajimoto R, Yoshizawa H, Kawano H, Kuwahara H, Tokura Y, Ohoyama K and Ohashi M 1999 *Phys. Rev.* B **60** 9506
[2] Urushibara A, Moritomo Y, Arima T, Asamitsu A, Kido G and Tokura Y 1995 *Phys. Rev.* B **51** 14103
[3] Schiffer P, Ramirez A P, Bao W and Cheong S-W 1995 *Phys. Rev. Lett.* **75** 3336
[4] Rao C N R and Raveau B 1998 *Colossal Magnetoresistance, Charge Ordering and Related Properties of Manganese Oxides* (Singapore: World Scientific) and references therein
[5] Rana D S, Markna J H, Parmar R N, Kuberkar D G, Raychaudhuri P, John J and Malik S K 2005 *Phys. Rev.* B **71** 212404
[6] Zhang J, Xu Y, Cao S, Cao G, Zhang Y and Jing C 2005 *Phys. Rev.* B **72** 054410
[7] Auslender M, Karkin A E, Rosenberg E and Gorodetsky G 2001 *J. Appl. Phys.* **89** 6639
[8] Argyriou D N, Bordallo H N, Campbell B J, Cheetham A K, Cox D E, Gardner J S, Hanif K, dos Santos A and Strouse G F 2000 *Phys. Rev.* B **61** 15269
[9] Chatterji T, McIntyre G J, Caliebe W, Suryanarayanan R, Dhalenne G and Revcolevschi A 2000 *Phys. Rev.* B **61** 570
[10] Ling C D, Millburn J E, Mitchell J F, Argyriou D N, Linton J and Bordallo H N 2000 *Phys. Rev.* B **62** 15096
[11] Chatterjee S, Chou P H, Chang C F, Hong I P and Yang H D 2000 *Phys. Rev.* B **61** 6106
[12] Hwang H Y, Cheong S-W, Radaelli P G, Marezio M and Batlogg B 1995 *Phys. Rev. Lett.* **75** 914
[13] Gordon I, Wagner P, Moshchalkov V V, Bruynseraede Y, Apostu M, Suryanarayanan R and Revcolevschi A 2001 *Phys. Rev.* B **64** 092408
[14] Yassin O A 2000 *PhD Theses* Indian Institute of Technology
[15] Cox D E, Radaelli P G, Marezio M and Cheong S-W 1998 *Phys. Rev.* B **57** 3305
[16] Seshadri R, Maignan A, Hervieu M, Nguyen N and Raveau B 1997 *Solid State Commun.* **101** 453
[17] Ibrahim H M, Yassin O A, de Châtel P F and Bhatia S N 2005 *Solid State Commun.* **134** 695
[18] Mott N F and Davis E A 1971 *Electronic Processes in Non-Crystalline Materials* (Oxford: Oxford University Press)
[19] Shlovski B I and Efros A L 1984 *Electronic Properties of Doped Semiconductors* (Berlin: Springer)
[20] Bhatia S N, Chowdhury P, Gupta S and Padalia B D 2002 *Phys. Rev.* B **66** 214523
[21] Moritomo Y, Nakamura A, Ohoyama K, Ohashi M and Hirota K 1999 *J. Phys. Soc. Japan* **68** 631
[22] Mitchell J F, Argyriou D N, Jorgensen J D, Hinks D G, Potter C D and Bader S D 1997 *Phys. Rev.* B **55** 63
[23] Coey J M D, Viret M and Ranno L 1995 *Phys. Rev. Lett.* **75** 3910
[24] Viret M, Ranno L and Coey J M D 1997 *Phys. Rev.* B **55** 8067
[25] Eto T, Sundaresan A, Honda F and Oomi G 2005 *Phys. Rev.* B **72** 060402(R)
[26] Moorjani K and Coey J M D (ed) 1984 *Magnetic Glasses* (Amsterdam: Elsevier)
[27] Nath T K and Majumdar A K 1997 *Phys. Rev.* B **55** 5554
[28] Altshuler B L and Aranov A G 1985 *Electron–Electron Interaction in Disordered Systems* ed A L Efros and M Pollak (New York: Elsevier)
[29] Lee P A and Ramakrishnan T V 1985 *Rev. Mod. Phys.* **57** 287
[30] Yamamoto K, Kimura T, Ishikawa T, Katsufuji T and Tokura Y 2000 *Phys. Rev.* B **61** 14706